Journal of Polymer Science

WILEY

JOURNAL OF POLYMER SCIENCE

RESEARCH ARTICLE

Viscoelastic Supramolecular Networks Based on Guanidinium-Oxyanion Interactions

Oliver G. Venablerose | Evan B. Van Pelt | Ava L. DeKoekkoek | Michael B. Larsen

Department of Chemistry, Western Washington University, Bellingham, Washington, USA

Correspondence: Michael B. Larsen (larsen32@wwu.edu)

Received: 13 January 2025 | **Revised:** 7 April 2025 | **Accepted:** 8 April 2025

Funding: This work was supported by the Division of Materials Research (2105149 and 2320809).

Keywords: charge-assisted hydrogen bonding | degradable materials | supramolecular polymers

ABSTRACT

We describe the synthesis and characterization of supramolecular networks based on charge-assisted hydrogen bonding interactions of guanidinium and oxyanion functionalities. Although they are constructed entirely of small-molecule components, these materials display properties such as a glass transition and time- and temperature-dependent viscoelastic rheological behavior. These properties can be tuned by the choice of each network component: T_g varies by over 50°C in the studied networks, and relaxation times scaled with changes to T_g. However, these supramolecular materials are inherently degradable and thermally reversible as no covalent macromolecular structure is formed.

1 | Introduction

An extended architecture of covalent bonds is a fundamental feature of polymeric materials that is responsible for many of their desirable characteristics. However, this macromolecular structure can also lead to environmental persistence, slow degradation, and challenges in reprocessing these materials; for example, less than 15% of plastic that is recycled returns to similar applications [1]. As a result, the global accumulation of polymer waste is an emergent crisis. The United Nations estimates that approximately 75% of all plastic produced since 1950 has become waste in landfills, in uncontrolled disposal streams, or dumped into the environment [2]. The problem is particularly pressing in marine ecosystems, where plastic has entered the sedimentary geologic record [3] and is projected to surpass the total mass of fish in the ocean by 2050 [1]. These issues are reflections of the macromolecular architecture of consumer polymers: as chains or networks composed of robust covalent bonds, they are challenging to break down to small molecules which can be more easily assimilated into the environment. Thus, substantial efforts have been made in the polymer science community to enhance the degradability of these materials. For example, the development of new, inherently biodegradable polymers is of much interest, as they may be able to naturally break down to innocuous small molecules under environmental conditions [4, 5]. Other strategies such as chemical recycling to monomer and self-immolative depolymerization aim to create circular processes in which macromolecules are deconstructed to their corresponding monomers and subsequently repolymerized to new materials, thus avoiding issues such as unwanted chain scission or crosslinking that may occur during traditional mechanical recycling [6–8].

The common goal of these approaches is the scission of covalent bonds in the macromolecular chain or network, ultimately transforming polymers back into small molecules. Alternatively, small molecules themselves can serve as the building blocks of supramolecular materials, which can be formed when percolating noncovalent interactions are of sufficient strength [9–12]. For example, cohesive bulk materials can arise from the assembly of small molecules through hydrogen bonding [13–16], metal–ligand coordination [17–19], and ionic interactions [20, 21]. Additionally, simple proton transfer reactions of multifunctional amines and carboxylic acids can create robust

supramolecular networks based on charge-assisted hydrogen bonds (CAHBs) [22], and previous work has demonstrated that these systems display polymer-like thermal and rheological properties (Figure 1a,b) [23–28].

Like amines, guanidines are nitrogenous bases capable of undergoing proton transfer reactions with oxyacids. However, they are more basic than amines and associate more strongly with oxyanions [29, 30]. For example, quantitative binding studies have determined equilibrium association constants (K_{assoc}) between guanidinium and carboxylate ions to be on the order of 10^3 in DMSO, varying based on the guanidinium *N*-substitution pattern [31]. For comparison, K_{assoc} of ammonium-carboxylate interactions is approximately 10^1 under similar conditions [32]. Additionally, guanidine-substituted small molecules bind more strongly to the phosphate functionalities in DNA compared to amine-substituted congeners [33]. These observations are broadly attributed to the ability of guanidines to form strong, bidentate CAHB interactions with three-center oxyanions such as carboxylates and phosphonates (Figure 1c) [34, 35]. A further benefit of this approach is that common synthetic routes to guanidines allow for substantial structural tuning of *N*-substituents. Therefore, we envisioned the combination of multifunctional guanidines and multifunctional oxyacids to be a versatile method for the preparation of robust supramolecular materials. Here, we present the synthesis and thermorheological characterization of a library of guanidinium-oxyanion networks based on CAHBs. These materials exhibit hallmark rheological features of polymer viscoelasticity such as power-law scaling in the low-frequency regime and a high-frequency plateau modulus, while their glass transition temperature (T_g) varies by over 50°C according to the molecular structure of each component. Additionally, we show that these materials can be recovered and reprocessed while maintaining their thermorheological properties.

2 | Results and Discussion

The bis(guanidines) used in this study (**bG1**–**bG4**, Figure 2) were prepared by nucleophilic addition of the corresponding amines to carbodiimides. While the use of diisopropyl carbodiimide to prepare **bG1** and **bG2** required heating in the presence of $Yb(OTf)_3$ for the reaction to occur [36], the addition of amines to *p*-tolyl carbodiimide to form **bG3** and **bG4** proceeded rapidly under ambient conditions, consistent with the relative electrophilicity of these species [37]. Supramolecular networks were formed by combining equimolar (with respect to functionalities) solutions of bis(guanidines) with a trifunctional oxyacid (**A1**–**A3**, Figure 2) and allowing the solvent to evaporate. Seven combinations of bis(guanidine) and oxyacid were chosen in order to investigate the effects of specific structural characteristics such as guanidine core structure, *N*-substitution, and oxyacid character on the thermorheological properties of the resulting networks. The materials were obtained as glassy solids or powders upon complete solvent removal. As controls, **bG1** was separately combined with trimethylolpropane (TMP) or trimethyl citrate (TMC), which contain three alcohol or three ester functionalities, respectively. The resulting materials can exhibit hydrogen bonding

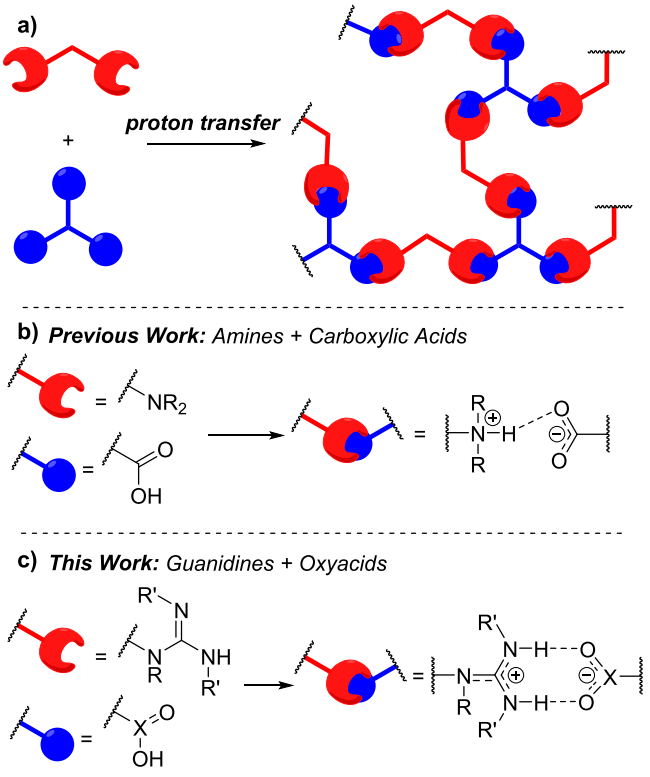

FIGURE 1 | (a) Proton transfer-induced supramolecular network formation between a multifunctional basic species (red) and multifunctional acidic species (blue); other $A_n + B_n$ combinations are also possible. (b) Previous work using amines and carboxylic acids. (c) This work using guanidines and oxyacids. R = H, alkyl; R′ = alkyl, aryl; X = C, P(OH).

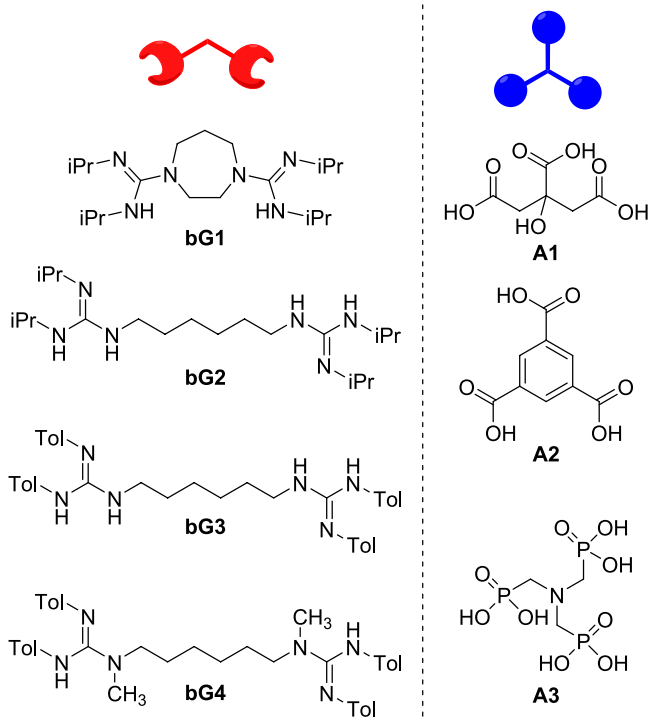

FIGURE 2 | Bis(guanidines) and trifunctional oxyacids used in this study. iPr = isopropyl; Tol = tolyl.

between their constituent components but lack the ability to undergo proton transfer reactions, preventing CAHB interactions in these cases. The ATR-IR spectra of each network made with an acidic component showed changes consistent with proton transfer reactions and extensive hydrogen bonding (Figures S1–S7). In particular, the absorptions attributed to C═N and (when present) C═O stretching frequencies largely shifted to lower wavenumbers compared to the starting bis(guanidines) and oxyacids, indicating formation of guanidinium–oxyanion pairs. Additionally, the appearance of a broad N–H absorption from ca. 2500–3500 cm^{-1} was consistent with substantial hydrogen bonding. The ATR-IR spectrum of control material **bG1-TMP** also showed some indications of hydrogen bonding such as shifting of C═N frequencies, but no broad N-H absorption was evident (Figure S8). Similarly, the spectrum of **bG1-TMC** did not show evidence of proton transfer reactions, as the C═O absorbance was unshifted compared to the starting component (Figure S9). Unlike covalent networks, the materials were also amenable to solution-phase characterization ^{1}H NMR spectroscopy revealed deshielding of protons adjacent to guanidinium functionalities relative to the corresponding signals in neutral bis(guanidines), consistent with proton transfer and formation of hydrogen bonded bis(guanidinium) species (Figures S10–S16). Consistent with its ATR-IR spectrum, the ^{1}H NMR spectrum of control **bG1-TMP** also showed signs of hydrogen bonding as evidenced by slight downfield shifting of the guanidine resonances compared to **bG1** itself (Figure S17). The ^{1}H NMR spectrum of **bG1-TMC** also indicated some solution-phase interactions due to similar shifting of guanidine resonances together with differentiation of protons in **TMC** that were previously magnetically equivalent (Figure S18).

Next, we probed the thermal properties of the materials by thermogravimetric analysis (TGA) and differential scanning calorimetry (DSC). TGA revealed modest thermal stability, as gauged by $T_{d,5\%}$ values of 170°C–216°C across materials (Figures S21–S25). We attribute this to the limited thermal stability of the guanidine components, as the precursors **bG1–bG4** tended to decompose at similar temperatures (Figures S26–S34). DSC provided further insight into the thermal properties of each material (Figures S35–S41). All networks displayed an endotherm characteristic of a glass transition, with T_g values dependent on both bis(guanidine) and oxyacid structure (Figure 3, Table 1). Networks made by combining **bG1** and **A1** displayed a reduced T_g (67°C) relative to the more rigid **bG1–A2** combination (T_g 132°C). The thermogram of **bG1–A2** also exhibited features between approximately 100°C and T_g that were not present in other formulations (Figure S36), possibly indicating a more complex morphology due to the rigid aromatic core of the tricarboxylic acid. As phosphonates bind guanidiniums more strongly compared to carboxylates, **bG1–A3** also displayed a higher T_g (108°C) compared to **bG1–A1**. Increasing the hydrogen bonding capacity by changing the guanidine to one bearing fewer alkyl substituents led to a higher T_g when combined with the same carboxylic acid (e.g., **bG1–A1** T_g 67°C, **bG2–A1** T_g 80°C). Substantial differences were also observed when *N*-isopropyl and *N*-tolyl substituents were exchanged. For example, networks of **bG2–A3** exhibited lower T_g than **bG3–A3** (111°C and 129°C, respectively). Finally, **bG4–A3** showed reduced T_g (94°C) compared to **bG3–A3** due to the diminished hydrogen

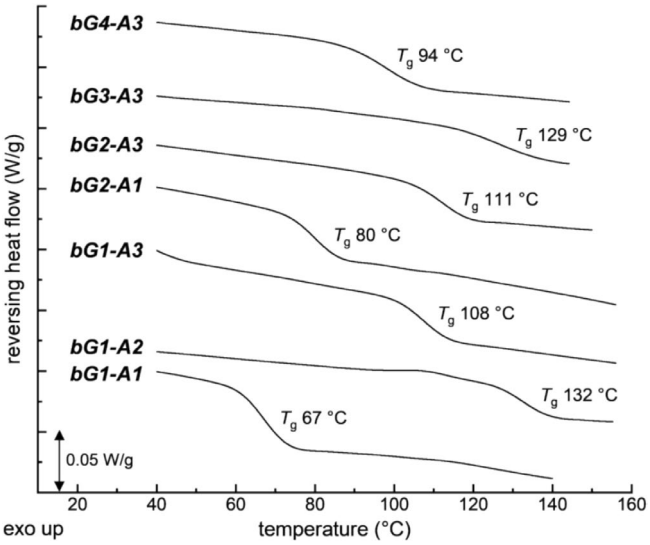

FIGURE 3 | Modulated DSC thermograms (reversing heat flow, second heat, exo up) of supramolecular networks with assigned T_g values. Data have been shifted vertically for clarity.

TABLE 1 | Compiled thermal and rheological characterization data of guanidinium-oxyanion supramolecular networks.

Network	T_g (°C)[a]	T_{nl} (°C)[b]	G′ (MPa)[c]	τ_{cross} (s)[d]
bG1–A1	67	70	3.3	4.9×10^{-3}
bG1–A2	132	120	3	8.0×10^{-4}
bG1–A3	108	130	9.2	2.4×10^{-3}
bG2–A1	80	83	6.2	1.5×10^{-2}
bG2–A3	111	128	1.6	1.1×10^{-1}
bG3–A3	129	137	4.4	2.7×10^{-3}
bG4–A3	94	102	2.1	6.0×10^{-3}

[a]Glass transition determined from modulated DSC (second heating cycle).
[b]Network-liquid transition temperature determined from modulus crossover in isochronal temperature ramps.
[c]Plateau modulus determined from SAOS frequency sweeps.
[d]Time at modulus crossover determined from frequency sweep master curves ($T_{ref} = T_g + 20 \pm 3$°C).

bonding capability of the tetrasubstituted guanidine in **bG4**, similar to the comparison of **bG1–A1** and **bG2–A1**. Overall, we found these properties to be quite reproducible; for instance, T_g varied by less than 10°C across independently synthesized iterations of **bG1–A1** (Figure S42). Importantly, the control materials **bG1–TMP** and **bG1–TMC**, which possessed only conventional hydrogen bonding interactions, did not show any thermal events indicative of glass transitions (Figures S43 and S44). Each small molecule precursor was also characterized by DSC (Figures S45–S47). In all cases, thermograms differed from corresponding supramolecular materials: some substances showed no discernible features in their thermograms, while others showed clear endotherms consistent with their known melting points. Even in cases where endotherms attributed to T_g were detected (e.g., **bG3** T_g 33°C, **bG4** T_g 20°C) they occurred at much lower temperatures than observed in corresponding supramolecular networks. These observations support the importance

of CAHBs in bringing about the thermal properties of these materials.

To understand the dynamic characteristics of these materials, we performed rheological analyses using small-amplitude oscillatory shear (SAOS) measurements. For each composition, isochronal temperature ramps at 6.28 rad s^{-1} indicated solid-like behavior at low temperatures, with $G'_2 > G''_3$ (Figures 4a and S48–S53). Continued heating resulted in a modulus crossover point ($G'_2 = G''_3$), identified in similar materials as the network-liquid transition temperature (T_{nl}) [23]. Comparison with values of T_g obtained by DSC reveals these thermal events to take place at similar temperatures in most network compositions (Table 1). Above T_{nl}, each material behaves as a viscoelastic liquid with $G''_3 > G'_2$, and no rubbery plateau is evident on this timescale. Thus, despite the multifunctional nature of the guanidinium and oxyanion components, no permanent crosslinks or entanglements exist in the material. This observation further supports CAHB interactions as being the primary governors of viscoelastic behavior.

We next conducted a series of isothermal frequency sweeps using SAOS measurements. To facilitate comparisons across networks, we constructed master curves using time–temperature superposition (TTS), with $T_{ref} = T_g + 20 \pm 3$°C. In all cases, $G' > G''$ at high frequencies, and a plateau in G' was also observed (Figures 4b and S54–S59). In typical polymers, this plateau reflects restricted chain motion due to covalent crosslinks and/or physical entanglements. Consistent with similar materials [25], we attribute the plateau in our guanidinium-oxyanion networks to CAHB interactions that restrict motion on this timescale. Accordingly, the molar mass between effective crosslinks as calculated from G' is much lower than in many covalent polymers (Table S1) [38], further supporting that no entanglements or covalent crosslinks exist in the material. Additionally, we estimated crosslink functionality by conducting ^{1}H NMR titration studies, which are routinely used in supramolecular chemistry to determine binding stoichiometry of two partners [39]. Consistent with previous work [31], titrations of a monofunctional guanidine with benzoic acid indicated a 1:1 binding stoichiometry (Figures S60 and S61, Table S2). Thus, we hypothesize the effective crosslink functionality of **A1–A3** to be equivalent to the number of acidic groups in each molecule.

Each master curve also displayed a crossover frequency where $G'_2 = G''_3$, which serves as an estimation of a relaxation time (τ_{cross}). At T_{ref}, all networks displayed τ_{cross} of approximately 10^{-1}–10^{-4} s (Table 1), which reflects the rapid timescale of noncovalent bond dynamics in the material. This provides additional evidence for these interactions underlying the observed viscoelastic behavior, though no discernible trends were evident across different network compositions. In the intermediate frequency regime below the modulus crossover, $G' < G''$ and thus each material behaved as a viscoelastic liquid. However, terminal relaxation was not observed in any composition, as the determined power law scalings ($G' \propto \omega^{1.11–1.82}$; $G'' \propto \omega^{0.86–0.98}$) deviated from those predicted for the terminal regime for Maxwell or Rouse models of viscoelasticity ($G' \propto \omega^2$; $G'' \propto \omega^1$) [40, 41]. Similar divergence is often observed in supramolecular polymers, as noncovalent interactions can alter dynamics in the intermediate- to low-frequency regimes and suppress terminal relaxation [42–44].

Finally, we explored the reprocessability and thermal reversibility of these materials using **bG1–A1** as a test case. Solution-phase ^{1}H NMR spectroscopy before and after processing and SAOS experiments exhibited no detectable molecular changes (Figure S62). Accordingly, T_{nl} changed by less than 4°C when the same sample was heated and cooled multiple times while in the rheometer (Figure 5). This rapid thermal reversibility is a hallmark of supramolecular polymers [24] and indicates that the viscoelastic characteristics of the material are maintained through multiple heating cycles with good reproducibility. Coupled with the batch-to-batch regularity of T_g values (Figure S42), we conclude that the thermorheological properties of these materials are relatively consistent for a given molecular composition.

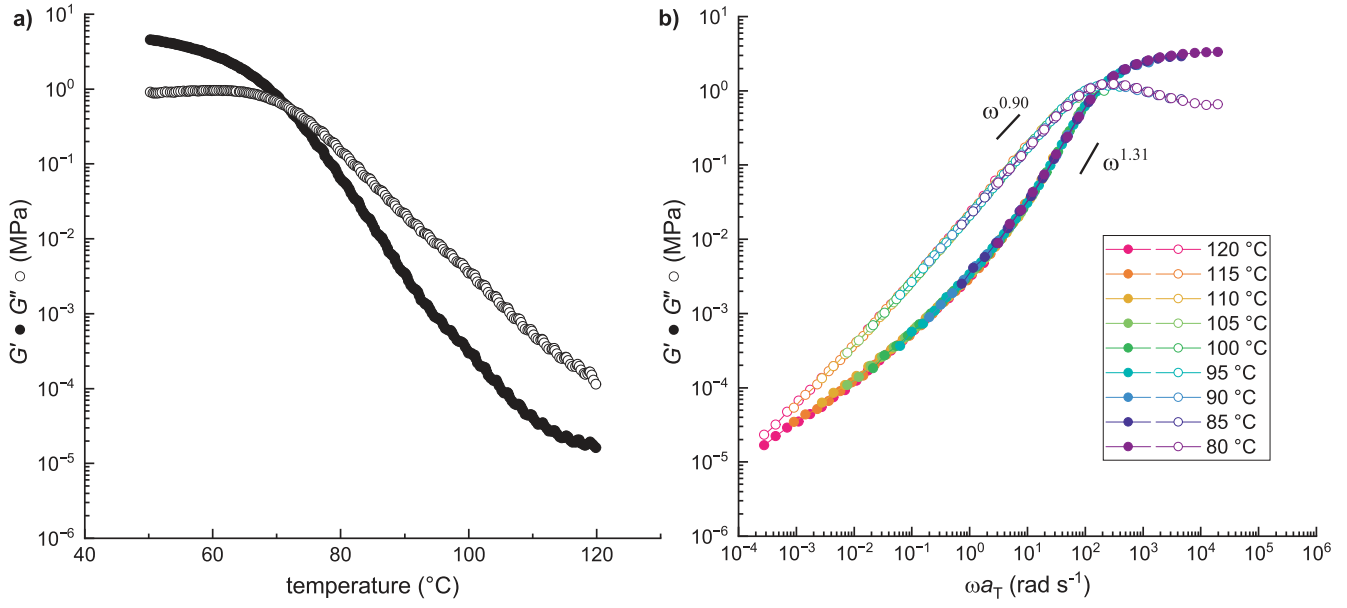

FIGURE 4 | (a) Isochronal temperature ramp (6.28 rad s^{-1}, 0.5% strain, 3°C min^{-1}) of **bG1–A1**. (b) Master curve constructed from SAOS frequency sweeps (0.5% strain, 0.01–100 Hz) of **bG1–A1**. T_{ref} = 95°C (T_g + 20°C). Power law scalings of loss and storage moduli are given for reference.

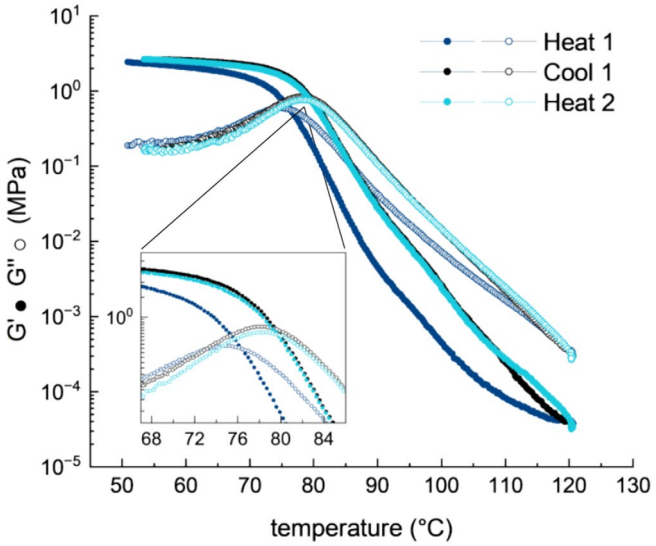

FIGURE 5 | Isochronal temperature ramps (6.28 rad s^{-1}, 0.5% strain, 3°C min^{-1}) of a single sample of **bG1–A1** heated, cooled, and heated a second time in succession. $T_{nl,heat\ 1}$ = 76.4°C, $T_{nl,cool\ 1}$ = 79.6°C, $T_{nl,heat\ 2}$ = 79.8°C.

3 | Conclusions

In conclusion, we have developed a new class of supramolecular networks composed entirely of small molecules. CAHB interactions between multifunctional guanidinium and oxyacid species lead to the formation of a cohesive material that displays characteristics such as a glass transition, high-frequency plateau modulus, and power-law scaling of moduli in the intermediate- to low-frequency regime. However, as no macromolecular chain architecture exists, the materials are inherently degradable and the network structure is thermally reversible. In the future, we hope to improve the thermal stability and reprocessability of these systems, develop molecular structure-thermorheological property relationships, and demonstrate the use of the guanidinium-oxyacid interaction in other realms of materials science.

4 | Experimental Section

4.1 | Materials

Unless otherwise noted, all chemicals were purchased from commercial sources and used as received. Dry tetrahydrofuran, dichloromethane, and toluene were obtained from an Inert PureSolv solvent purification system. *p*-Tolyl carbodiimide and **G1** were prepared as previously described [45, 46].

4.2 | Instrumentation

^{1}H and ^{13}C NMR spectra were recorded on a Bruker Avance III 500 MHz FT-NMR spectrometer. Chemical shifts are reported in delta (δ) units, expressed in parts per million (ppm) downfield from tetramethylsilane using the residual protio-solvent as an internal standard ($CDCl_3$, ^{1}H: 7.26 ppm and ^{13}C: 77.06 ppm; DMSO-d_6, ^{1}H: 2.50 ppm and ^{13}C 39.53 ppm; methanol-d_4 ^{1}H: 3.31 ppm and ^{13}C: 49.00 ppm). Coupling constants (J) are reported in Hz. MS analysis was performed with an Agilent 6545XT LC/Q-TOF spectrometer in positive polarity. IR spectroscopy was performed with a Thermo iS10 FT-IR with single-bounce diamond ATR. Thermogravimetric analyses (TGA) were performed on a TA Instruments Discovery 5500 with a platinum pan. Ramp experiments used a Hi Resolution dynamic procedure under nitrogen flow (40 mL/min), heating at a rate of 50.0°C/min to a final temperature of 700°C. Modulated DSC experiments were performed in aluminum sample pans on a TA Instruments Discovery X3. Modulated experiments were equilibrated at 0.00°C and held at isotherm for 10.0 min. Modulation consisted of an amplitude of 0.800°C and a period of 60.0 s with a ramp rate of 5.00°C/min. Two heat cycles to 175°C and one cool cycle to 0.00°C were completed under nitrogen flow (50 mL/min). Rheological analyses were performed on a TA Instruments DHR-2 Discovery Hybrid Rheometer using a 25 mm parallel plate geometry. For isochronal temperature ramp experiments, samples were deformed at 0.5% strain and 1.0 Hz and ramped at 3.0°C/min for the given temperature range. For frequency sweep experiments, samples were conditioned for a soak time of 60.0 s followed by the application of 0.5% strain from 0.01 to 100.0 Hz at each temperature. For both temperature ramp and frequency sweep experiments, non-iterative sampling was utilized to control strain, set to torque of 7.0 μM m.

4.3 | Experimental Procedures

4.3.1 | Synthesis of bG1

In an oven-dried flask cooled to 0°C, homopiperazine (0.400 g, 3.99 mmol, 1.00 equiv.) and ytterbium (III) trifluoromethanesulfonate (0.099 g, 0.160 mmol, 0.040 equiv.) were combined and placed under N_2. The flask was heated to 80°C, which formed a homogenous solution. Using an N_2-purged syringe, *N*,*N*′-diisopropylcarbodiimide (1.26 mL, 7.99 mmol, 2.00 equiv.) was added, and the reaction was stirred for 24 h at 80°C. The reaction mixture was cooled to ambient temperature, dissolved in dichloromethane (120 mL) and washed 3× with distilled water (10 mL portions). The resulting organic layer was dried with anhydrous sodium sulfate, and solvent was removed in vacuo. The crude product was purified by recrystallization in toluene to remove crystalline 1,3-diisopropylurea. After cooling, the crystalline urea was collected using vacuum filtration, and the filtrate was concentrated in vacuo. The resulting residue was dried on a Schlenk line under high vacuum at 60°C to yield **bG1** as a clear, off-yellow viscous oil (0.647 g, 46%). ^{1}H NMR (500 MHz, MeOD-d_4) δ 3.58 (hept, J = 6.4 Hz, 4H), δ 3.48 (s, 4H), 3.46–3.41 (m, 4H), 1.92–1.88 (m, 2H), 1.17 (d, J = 6.6 Hz, 24H). ^{13}C NMR (126 MHz, DMSO-d_6) δ 154.2, 50.0, 48.1, 46.0, 28.6, 24.4. MS (ESI): $[M + H^+]$ calc'd for $C_{19}H_{41}N_6$ 353.3393, found 353.3444.

4.3.2 | Synthesis of bG2

In an oven-dried flask, 1,6-diaminohexane (1.00 g, 8.61 mmol, 1.00 equiv.) and ytterbium (III) trifluoromethanesulfonate (0.213 g, 0.344 mmol, 0.040 equiv.) were combined and placed under N_2. The flask was heated to 60°C, which formed a homogenous solution. Using an N_2-purged syringe, *N*,*N*′-diisopropylcarbodiimide

(2.65 mL, 17.2 mmol, 2.00 equiv.) was added and the reaction was stirred for 3 h at 60°C. The reaction mixture was cooled to ambient temperature, dissolved in dichloromethane (100 mL) and washed 3× with distilled water (10 mL portions). The resulting organic layer was dried with anhydrous sodium sulfate and solvent was removed in vacuo. The crude product was dissolved in a solvent mixture of acetone and hexanes (25:75 v/v, 15 mL), cooled to 0°C for 24 h, and filtered with a 0.45 μm PTFE membrane filter. This process was completed a second time, and solvent was removed in vacuo followed by drying on a Schlenk line on high vacuum at 60°C to yield **bG2** as an off-white tacky solid (0.805 g, 25%). ^{1}H NMR (500 MHz, MeOD-d_4) δ 3.78 (hept, J = 6.4 Hz, 4H), 3.20 (t, J = 7.3 Hz, 4H), 1.69–1.53 (m, 4H), 1.47–1.36 (m, 4H), 1.23 (d, J = 6.4 Hz, 24H). ^{13}C NMR (126 MHz, MeOD) δ 154.6, 45.3, 43.2, 30.5, 27.8, 23.0. MS (ESI): [M + H$^+$] calc'd for $C_{20}H_{45}N_6$ 369.3706, found 369.3752.

4.3.3 | Synthesis of bG3

In an oven-dried flask, *p*-tolyl carbodiimide (0.200 g, 0.900 mmol, 2.00 equiv.) was dissolved in methanol (10 mL). To this solution, 1,6-diaminohexane (0.052 g, 0.450 mmol, 1.00 equiv.) was added and the reaction mixture was stirred at ambient temperature for 1 h while monitoring via TLC (95:5 v/v hexanes/ethyl acetate). Upon full carbodiimide conversion, the solvent was removed in vacuo and the remaining residue was precipitated in DI water. The solution was decanted and the solids dried on a Schlenk line on high vacuum at 50°C to give **bG3** as a white tacky solid (0.166 g, 66%). ^{1}H NMR (500 MHz, MeOD-d_4) δ 7.05 (d, J = 7.8 Hz, 8H), 6.92 (d, J = 7.8 Hz, 8H), 3.18 (t, J = 7.1 Hz, 4H), 2.25 (s, 12H), 1.61–1.47 (m, 4H), 1.39–1.26 (m, 4H). ^{13}C NMR (126 MHz, $CDCl_3$) δ 148.8, 130.0, 123.4, 41.6, 29.6, 26.8, 20.8. MS (ESI): [M + H$^+$] calc'd for $C_{36}H_{45}N_6$ 561.3706, found 561.3748.

4.3.4 | Synthesis of bG4

In an oven-dried flask, *p*-tolyl carbodiimide (2.56 g, 11.51 mmol, 2.00 equiv.) was dissolved in dry THF (64 mL). To this solution, *N,N′*-dimethyl-1,6-diaminohexane (1.00 mL, 5.76 mmol, 1.0 equiv.) was added and the reaction mixture was stirred at ambient temperature for 2 h while monitoring via TLC (95:5 v/v hexanes/ethyl acetate). Upon full carbodiimide conversion, the solvent was removed in vacuo and the remaining residue was triturated with DI water. The solution was decanted and the residue dried on a Schlenk line on high vacuum at 50°C to give **bG4** as a clear viscous oil (1.60 g, 47%). ^{1}H NMR (500 MHz, MeOD-d_4) δ 6.93 (d, J = 8.4 Hz, 8H), 6.70 (d, J = 8.4 Hz, 8H), δ 3.18 (t, J = 7.3 Hz, 4H), 2.88 (s, 6H), 2.19 (s, 12H), 1.56–1.50 (m, 4H), δ 1.25–1.22 (m, 4H). ^{13}C NMR (126 MHz, MeOD-d_4) δ 155.2, 132.2, 130.5, 121.5, 51.4, 36.5, 28.3, 27.4, 20.8. MS (ESI): [M + H$^+$] calc'd for $C_{38}H_{49}N_6$ 589.4019, found 589.4093.

4.3.5 | General Procedure for Supramolecular Network Synthesis (bG1–A1, bG1–A2, bG1–A3, bG2–A1)

To individual culture tubes, the desired bis(guanidine) (1.5 equiv., 3.0 equiv. guanidine functionality) and acid (1.0 equiv., 3.0 equiv. acidic functionality) were dissolved in compatible solvents. The two solutions were combined in a Pyrex petri dish and left to evaporate over 24 h under ambient conditions. The resulting supramolecular networks were collected and dried on a Schlenk line on high vacuum at 60°C. Note that integrations of signals in ^{1}H NMR spectra arising from the oxyanion component are 2/3 of the values expected from the corresponding structure due to differences in molecular stoichiometry of the bis(guanidine) versus acid in the initial loading.

4.3.6 | Synthesis of Supramolecular Network bG1–A1

Methanol (20 mL combined) was used to dissolve **bG1** (1.31 g, 3.71 mmol) and citric acid (0.47 g, 2.47 mmol) to yield **bG1–A1** as a white powdered solid (1.46 g, 82%). ^{1}H NMR (500 MHz, MeOD-d_4) δ 3.78 (s, 4H), 3.73 (hept, J = 6.4 Hz, 4H), 3.67–3.64 (m, 4H), 2.79 (d, J = 15.1 Hz, 1.3H), 2.74 (d, J = 15.1 Hz, 1.3H), 2.13–2.09 (m, 2H), 1.31 (d, J = 6.4 Hz, 24 H).

4.3.7 | Synthesis of Supramolecular Network bG1-A2

Methanol (11 mL combined) was used to dissolve 1,3,5-benzenetricarboxylic acid (0.31 g, 1.46 mmol) and **bG1** (0.82 g, 2.18 mmol) to yield **bG1–A2** as a white powdered solid (1.09 g, 97%). ^{1}H NMR (500 MHz, MeOD-d_4) δ 8.63 (s, 2H), 3.74–3.68 (m, 8H), 3.65–3.54 (m, 4H), 2.10–2.05 (m, 2H), 1.27 (d, J = 6.4 Hz, 24H).

4.3.8 | Synthesis of Supramolecular Network bG1–A3

Methanol (10 mL combined) was used to dissolve **bG1** (0.60 g, 1.70 mmol) and nitrilotris(methylene)triphosphonic acid (2.2 M aqueous solution, 0.52 mL, 1.14 mmol) to yield **bG1-A3** as a white powdered solid (0.95 g, 98%). ^{1}H NMR (500 MHz, MeOD-d_4) δ 3.81–3.72 (m, 8H), 3.71–3.65 (m, 4H), 3.39 (d, J = 10.5 Hz, 4H), 2.18–2.09 (m, 2H), 1.31 (d, J = 6.1 Hz, 24H).

4.3.9 | Synthesis of Supramolecular Network bG2-A1

Methanol (8.4 mL total) was used to dissolve **bG2** (0.72 g, 1.70 mmol) and citric acid (0.22 g, 1.14 mmol) to yield **bG2–A1** as a white powdered solid (0.90 g, 96%). ^{1}H NMR (500 MHz, MeOD-d_4) δ 3.83 (hept, J = 6.2 Hz, 4H), 3.26 (t, J = 7.3 Hz, 4H), 2.88 (d, J = 15.2 Hz, 1.3H), 2.77 (d, J = 15.1 Hz, 1.3H), 1.68–1.57 (m, 4H), 1.46–1.36 (m, 4H), 1.25 (d, J = 6.4 Hz, 24H).

4.3.10 | Synthesis of Supramolecular Network bG2–A3

Methanol (6 mL total) was used to dissolve **bG2** (0.24 g, 0.664 mmol) and nitrilotris(methylene)triphosphonic acid (2.2 M aqueous solution, 0.20 mL, 0.442 mmol) to yield **bG2–A3** as a clear glassy solid (0.36 g, 96%). ^{1}H NMR (500 MHz, MeOD-d_4) δ 3.84 (hept, J = 6.4 Hz, 4H), 3.27 (t, J = 7.3 Hz, 4H), 3.11 (d, J = 8.7, 4H), 1.66–1.60 (m, 4H), 1.45–1.39 (m, 4H), 1.26 (d, J = 6.4 Hz, 24H).

4.3.11 | Synthesis of Supramolecular Network bG3–A3

In a vial, **bG3** (1.4 g, 2.50 mmol) was combined with nitrilotris(methylene)triphosphonic acid (2.2 M aqueous solution, 0.76 mL, 1.66 mmol) and left to stir at ambient temperature for 48 h. Residual water was removed under direct airflow and the remaining residue was dried on a Schlenk line on high vacuum at 60°C to yield **bG3–A3** as an off-white powdered solid (1.75 g, 92%). ^{1}H NMR (500 MHz, MeOD-d_4) δ 7.06 (d, J = 8.1 Hz, 8H), 7.01 (d, J = 8.1 Hz, 8H), 3.29–3.17 (m, 6H), 2.24 (s, 12H), 1.70–1.59 (m, 4H), 1.44–1.36 (m, 4H).

4.3.12 | Synthesis of Supramolecular Network bG4–A3

To individual culture tubes, a 10:4.5 v/v dimethylformamide:DI water solution (2.3 mL) was used to dissolve **bG4** (0.47 g, 0.79 mmol), and dimethylformamide (0.92 mL) was combined with nitrilotris(methylene)triphosphonic acid (2.2 M aqueous solution, 0.24 mL, 0.53 mmol). The two solutions were combined in a vial and stirred at ambient temperatures for 24 h. Residual solvent was removed under direct airflow and the residue was dried on a Schlenk line on high vacuum at 60°C to yield **bG4–A3** as a white powdered solid (0.57 g, 91%) [1].H NMR (500 MHz, MeOD-d_4) δ 7.02 (d, J = 8.6 Hz, 8H), 6.97 (d, J = 8.6 Hz, 8H), 3.44 (t, J = 7.4 Hz, 4H), 3.10 (s, 6H), 3.06–3.03 (m, 3H), 2.21 (s, 12H), 1.70–1.67 (m, 4H), 1.34–1.32 (m, 4H).

4.3.13 | General Procedure for Preparation of Rheological Samples

Rheological samples were prepared using an MSE PRO (25.4 mm) pressing die set and a benchtop Carver press (3851-0). The supramolecular networks were first processed with a mortar and pestle to a fine powder. 0.50 g of sample was then added to the die that had been pre-treated with a thin layer of PTFE spray. Four tons of axial force were applied at ambient temperatures for 15 min. The mold was rotated 180° axially, and again 4 tons of axial force were applied at ambient temperatures for an additional 15 min.

4.3.14 | General Procedure for Reprocessing Studies

After rheological studies were conducted, **bG1–A1** was removed from the rheometer plates and dissolved in methanol. The solution was then transferred to a vial and the solvent was removed in vacuo. The recovered network was then dried on a Schlenk line under high vacuum at 60°C, followed by characterization and/or sample processing as described above.

4.3.15 | Procedure for ^{1}H NMR Titration Experiments

A 3.00 mL **Host** solution of **G1** (21.0 mg, 0.0227 mM) in potassium carbonate-treated $CDCl_3$ was prepared. A 1.00 mL portion of the **Host** solution was combined with benzoic acid (55.5 mg, 0.454 mM) to prepare the **Guest** solution. A 0.50 mL portion of the **Host** solution was placed into an NMR sample tube. Spectra were collected after each subsequent addition of **Guest** (5.0 μL, 0.20 equiv. benzoic acid vs.**G1**), ranging from 0.0 equiv. [**Guest**] to 2.0 equiv. [**Guest**]. A total of 11 spectra were gathered for each trial, and a total of 3 trials were conducted. Break points for each trial were found by extrapolating linear fits of the 0.0 to 0.8 equiv. [**Guest**] region and the 1.2–2.0 equiv. [**Guest**] region and finding the intersection of the two fits.

Acknowledgments

We acknowledge the National Science Foundation for support of this research (DMR 2105149). Portions of this work were carried out using instrumentation supported by the National Science Foundation (MRI 2320809). The authors thank Kyle Mikkelsen for help in thermorheological analysis.

Conflicts of Interest

The authors declare no conflicts of interest.

Data Availability Statement

The data supporting this article have been included as part of the Supporting Information.

References

1. Ellen MacArthur Foundation, "The New Plastics Economy: Rethinking the Future of Plastics," 2016, accessed August 29, 2023, https://ellenmacarthurfoundation.org/the-new-plastics-economy-rethinking-the-future-of-plastics.

2. United Nations Environment Programme, "From Pollution to Solution: A Global Assessment of Marine Litter and Plastic Pollution," 2021, accessed August 29, 2023, https://wedocs.unep.org/bitstream/handle/20.500.11822/36963/POLSOL.pdf.

3. J. A. Brandon, W. Jones, and M. D. Ohman, "Multidecadal Increase in Plastic Particles in Coastal Ocean Sediments," *Science Advances* 5 (2019): eaax0587.

4. P. Tyagi, S. Agate, O. D. Velev, L. Lucia, and L. Pal, "A Critical Review of the Performance and Soil Biodegradability Profiles of Biobased Natural and Chemically Synthesized Polymers in Industrial Applications," *Environmental Science & Technology* 56 (2022): 2071–2095.

5. T. P. Haider, C. Völker, J. Kramm, K. Landfester, and F. R. Wurm, "Plastics of the Future? The Impact of Biodegradable Polymers on the Environment and Society," *Angewandte Chemie, International Edition* 58 (2019): 50–62.

6. G. W. Coates and Y. D. Y. L. Getzler, "Chemical Recycling to Monomer for an Ideal, Circular Polymer Economy," *Nature Reviews Materials* 5, no. 7 (2020): 501–516, https://doi.org/10.1038/s41578-020-0190-4.

7. Y. Liu and X.-B. Lu, "Emerging Trends in Closed-Loop Recycling Polymers: Monomer Design and Catalytic Bulk Depolymerization," *Chemistry—A European Journal* 29 (2023): e202203635.

8. S. Yang, S. Du, J. Zhu, and S. Ma, "Closed-Loop Recyclable Polymers: From Monomer and Polymer Design to the Polymerization-Depolymerization Cycle," *Chemical Society Reviews* 53 (2024): 9609–9651.

9. L. Brunsveld, B. J. B. Folmer, E. W. Meijer, and R. P. Sijbesma, "Supramolecular Polymers," *Chemical Reviews* 101 (2001): 4071–4098.

10. T. F. A. De Greef, M. M. J. Smulders, M. Wolffs, A. P. H. J. Schenning, R. P. Sijbesma, and E. W. Meijer, "Supramolecular Polymerization," *Chemical Reviews* 109 (2009): 5687–5754.

11. T. Aida and E. W. Meijer, "Supramolecular Polymers—We've Come Full Circle," *Israel Journal of Chemistry* 60, no. 1–2 (2020): 33–47, https://doi.org/10.1002/ijch.201900165.

12. J. D. Fox and S. J. Rowan, "Supramolecular Polymerizations and Main-Chain Supramolecular Polymers," *Macromolecules* 42 (2009): 6823–6835.

13. P. Cordier, F. Tournilhac, C. Soulié-Ziakovic, and L. Leibler, "Self-Healing and Thermoreversible Rubber From Supramolecular Assembly," *Nature* 451 (2008): 977–980.

14. R. P. Sijbesma, F. H. Beijer, B. J. B. Folmer, et al., "Reversible Polymers Formed From Self-Complementary Monomers Using Quadruple Hydrogen Bonding," *Science* 278 (1997): 1601–1604.

15. C. Fouquey, J.-M. Lehn, and A.-M. Levelut, "Molecular Recognition Directed Self-Assembly of Supramolecular Liquid Crystalline Polymers From Complementary Chiral Components," *Advanced Materials* 2 (1990): 254–257.

16. C. B. St. Pourcain and A. C. Griffin, "Thermoreversible Supramolecular Networks With Polymeric Properties," *Macromolecules* 28, no. 12 (1995): 4116–4121, https://doi.org/10.1021/ma00116a010.

17. S. Kelch and M. Rehahn, "High-Molecular-Weight Ruthenium(II) Coordination Polymers: Synthesis and Solution Properties," *Macromolecules* 30 (1997): 6185–6193.

18. W. C. Yount, H. Juwarker, and S. L. Craig, "Orthogonal Control of Dissociation Dynamics Relative to Thermodynamics in a Main-Chain Reversible Polymer," *Journal of the American Chemical Society* 125 (2003): 15302–15303.

19. A. J. Boydston, K. A. Williams, and C. W. Bielawski, "A Modular Approach to Main-Chain Organometallic Polymers," *Journal of the American Chemical Society* 127 (2005): 12496–12497.

20. M. Wathier and M. W. Grinstaff, "Synthesis and Properties of Supramolecular Ionic Networks," *Journal of the American Chemical Society* 130 (2008): 9648–9649.

21. M. A. Aboudzadeh, M. E. Muñoz, A. Santamaría, and D. Mecerreyes, "New Supramolecular Ionic Networks Based on Citric Acid and Geminal Dicationic Ionic Liquids," *RSC Advances* 3, no. 23 (2013): 8677–8682, https://doi.org/10.1039/c3ra40629f.

22. S. J. Grabowski, "What Is the Covalency of Hydrogen Bonding?," *Chemical Reviews* 111 (2011): 2597–2625.

23. M. A. Aboudzadeh, M. E. Muñoz, A. Santamaría, R. Marcilla, and D. Mecerreyes, "Facile Synthesis of Supramolecular Ionic Polymers That Combine Unique Rheological, Ionic Conductivity, and Self-Healing Properties," *Macromolecular Rapid Communications* 33 (2012): 314–318.

24. M. A. Aboudzadeh, M. E. Muñoz, A. Santamaría, M. J. Fernández-Berridi, L. Irusta, and D. Mecerreyes, "Synthesis and Rheological Behavior of Supramolecular Ionic Networks Based on Citric Acid and Aliphatic Diamines," *Macromolecules* 45 (2012): 7599–7606.

25. A. Aboudzadeh, M. Fernandez, M. E. Muñoz, A. Santamaría, and D. Mecerreyes, "Ionic Supramolecular Networks Fully Based on Chemicals Coming From Renewable Sources," *Macromolecular Rapid Communications* 35 (2014): 460–465.

26. W. Yang, F. Liu, R. Li, X. Wang, and W. Hao, "Multiple Stimuli-Responsive Fluorescent Sensor From Citric Acid and 1-(2-Aminoethyl) piperazine," *ACS Applied Materials & Interfaces* 10 (2018): 9123–9128.

27. L. I. Ronco, G. C. Luque, C. A. Calderón, et al., "Biobased Supramolecular Ionic Networks With Optimized Crystallinity and Mechanical Properties as Promising Dynamic Materials for Eutectogels Design," *Materials Today Chemistry* 30 (2023): 101525.

28. Y. Cheng, E. Hirano, H. Wang, et al., "Mechanically Strong Yet Metabolizable Supramolecular Plastics by Desalting Upon Phase Separation," *Science* 386, no. 6724 (2024): 875–881, https://doi.org/10.1126/science.ado1782.

29. B. Springs and P. Haake, "Equilibrium Constants for Association of Guanidinium and Ammonium Ions With Oxyanions: The Effect of Changing Basicity of the Oxyanion," *Bioorganic Chemistry* 6 (1977): 181–190.

30. N. Sakai and S. Matile, "Anion-Mediated Transfer of Polyarginine Across Liquid and Bilayer Membranes," *Journal of the American Chemical Society* 125 (2003): 14348–14356.

31. B. Linton and A. D. Hamilton, "Calorimetric Investigation of Guanidinium-Carboxylate Interactions," *Tetrahedron* 55 (1999): 6027–6038.

32. J. Zielińska, M. Makowski, K. Maj, A. Liwo, and L. Chmurzyński, "Acid–Base and Hydrogen-Bonding Equilibria in Aliphatic Amine and Carboxylic Acid Systems in Non-Aqueous Solutions," *Analytica Chimica Acta* 401 (1999): 317–321.

33. K. Ohara, M. Smietana, A. Restouin, et al., "Amine-Guanidine Switch: A Promising Approach to Improve DNA Binding and Antiproliferative Activities," *Journal of Medicinal Chemistry* 50 (2007): 6465–6475.

34. W. Wang, J. Gu, X. Zou, W. Tong, and H. Gong, "Solid State Studies of the Assembly of Diionic Guanidinium/Carboxylate Compounds," *Tetrahedron Letters* 56 (2015): 2684–2687.

35. K. A. Schug and W. Linder, "Noncovalent Binding Between Guanidinium and Anionic Groups: Focus on Biological and Synthetic-Based Arginine/Guanidinium Interactions With Phosph(On)ate and Sulf(On)ate Residues," *Chemical Reviews* 105 (2005): 67–114.

36. X. Zhu, Z. Du, F. Xu, and Q. Shen, "Ytterbium Triflate: A Highly Active Catalyst for Addition of Amines to Carbodiimides to N,N2,N3-Trisubstituted Guanidines," *Journal of Organic Chemistry* 74 (2009): 6347–6349.

37. Z. Li, R. J. Mayer, A. R. Ofial, and H. Mayr, "From Carbodiimides to Carbon Dioxide: Quantification of Electrophilic Reactivities of Heteroallenes," *Journal of the American Chemical Society* 142 (2020): 8383–8402.

38. L. J. Fetters, D. J. Lohse, D. Richter, T. A. Witten, and A. Zirkel, "Connection Between Polymer Molecular Weight, Density, Chain Dimensions, and Melt Viscoelastic Properties," *Macromolecules* 27 (1994): 4639–4647.

39. P. Thordarson, "Determining Association Constants From Titration Experiments in Supramolecular Chemistry," *Chemical Society Reviews* 40 (2011): 1305–1323.

40. P. C. Heimenz and T. P. Lodge, *Polymer Chemistry*, 2nd ed. (CRC Press, 2007), 419–439.

41. R. G. Ricarte and S. Shanbhag, "A Tutorial Review of Linear Rheology for Polymer Chemists: Basics and Best Practices for Covalent Adaptable Networks," *Polymer Chemistry* 15 (2024): 815–846.

42. M. Golkaram and K. Loos, "A Critical Approach to Polymer Dynamics in Supramolecular Polymers," *Macromolecules* 52 (2019): 9427–9444.

43. A. Shabbir, H. Goldansaz, O. Hassager, E. van Ruymbeke, and N. J. Alvarez, "Effect of Hydrogen Bonding on Linear and Nonlinear Rheology of Entangled Polymer Melts," *Macromolecules* 48 (2015): 5988–5996.

44. S. Seiffert, "Effect of Supramolecular Interchain Sticking on the Low-Frequency Relaxation of Transient Polymer Networks," *Macromolecular Rapid Communications* 37 (2016): 257–264.

45. A. J. Melchor Bañales and M. B. Larsen, "Thermal Guanidine Metathesis for Covalent Adaptable Networks," *ACS Macro Letters* 9 (2020): 937–943.

46. V. Ramirez, E. B. Van Pelt, R. K. Pooni, A. J. Melchor Bañales, and M. B. Larsen, "Thermodynamic, Kinetic, and Mechanistic Studies of the Thermal Guanidine Metathesis Reaction," *Organic & Biomolecular Chemistry* 20, no. 29 (2022): 5861–5868, https://doi.org/10.1039/d2ob01036d.

Supporting Information

Additional supporting information can be found online in the Supporting Information section.